Total Harmonic Distortion Measurement System of Electronic Devices up to 100 MHz With Remarkable Sensitivity

Takanori Komuro, *Member, IEEE*, Shingo Sobukawa, Hiroshi Sakayori, Masashi Kono, *Student Member, IEEE*, and Haruo Kobayashi, *Member, IEEE*

***Abstract*—This paper describes a system for measuring total harmonic distortion (THD) signal components between 1 and 100 MHz at levels down to −130 dBc, which has not been previously achieved. This system consists of mechanically sturdy passive bandpass (BPF) and passive band-elimination (BEF) filters with carefully selected parts. The BPF is used to create a pure sinusoidal signal input to the device under test, whereas the BEF removes the fundamental frequency component of the output signal to overcome dynamic range limitations of a spectrum analyzer that is used to measure the output. We describe design concepts and implementation of these filters, as well as measurement results that show the performance achieved. We also propose to use our BPF to provide a pure sine wave output from signal generators that use analog-to-digital converters (ADCs) as the signal source. A high-precision THD measuring system can be used to measure the ac linearity of electronic devices (such as operational amplifiers, ADCs, and digital-to-analog converters) that operate at frequencies up to several tens of megahertz.**

***Index Terms*—Analog circuit, automatic test equipment, band elimination filter (BEF), bandpass filter (BPF), distortion, harmonics, large-scale integration (LSI) testing, total harmonic distortion (THD) measurement.**

I. Introduction

MEASUREMENT of the total harmonic distortion (THD) of electronic devices has a long history; for audio systems, a THD figure is used as a representation of ac linearity [1]. THD measuring equipment for audio frequencies (up to 100 kHz) is readily available commercially [2], [3], and active filter technology can be used in such equipment. On the other hand, in the past, typical systems that operate at frequencies of several megahertz were radio-frequency (RF) systems that employ heterodyne technology; in such applications, harmonic distortion of the signal is of less interest than in the aforementioned audio example because RF applications are more concerned with just the narrow band of modulation (and intermodulation) components around the carrier (Fig. 1). However, recent progress in semiconductor technology has led to a proliferation of wideband applications with baseband frequency components of several megahertz, like xDSL, cellular phone baseband signals, and high-definition video (Fig. 1). For such applications, the THD is a good index for representing the linearity characteristics of analog circuits [like operational amplifiers, analog-to-digital converters (ADCs), and digital-to-analog converters (DACs)] [4]. However, for THD testing of wideband devices over a wide dynamic range, it is very difficult to use the active filter technology to measure THD components that are 100 dB below the carrier because of linearity and noise limitations of active circuits. Currently, there are no precision THD measuring instruments for equipment with baseband signal frequencies of several megahertz.

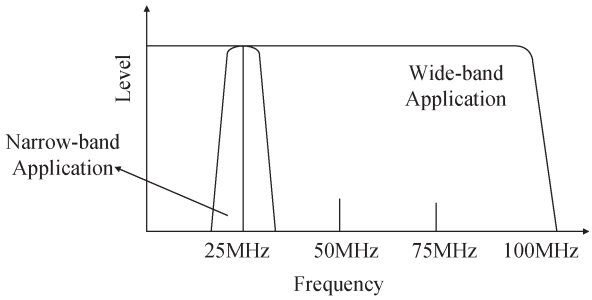

Fig. 1. Signal bands for narrow-band and wideband applications.

In this paper, we propose a system for measuring very small THD signal components (down to levels of −130 dBc) over a wide frequency range (1–100 MHz), and we have implemented this system and validated its performance. The system consists of a passive bandpass filter (BPF) and a passive band-elimination filter (BEF). The passive BPF is used to create a pure sine wave input to the device under test (DUT). The passive BEF is used to remove the fundamental frequency component from the DUT output signal without affecting the levels of harmonics so that the following spectrum analyzer can detect the harmonics with high precision. The filters are built with selected passive elements (L, C, R) for good linearity and noise performance. Section II describes the design concepts, and Section III shows typical THD measurement results, which validate the effectiveness of our proposed method. Finally, Section IV provides conclusions.

Here, we define the THD of an electronic device, as well as the unit of decibels relative to carrier (dBc) as follows. If we

Manuscript received May 22, 2006; revised January 4, 2007.

T. Komuro and H. Sakayori are with Agilent Technology International, Hachioji 192-0033, Japan.

S. Sobukawa is with NF Corporation, Yokohama 223-8508, Japan.

M. Kono and H. Kobayashi are with Gunma University, Kiryu 376-8515, Japan.

Color versions of one or more of the figures in this paper are available online at http://ieeexplore.ieee.org.

Digital Object Identifier 10.1109/TIM.2007.904548

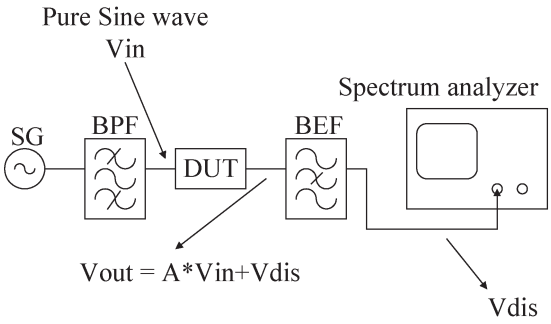

Fig. 2. Block diagram of our THD measurement system.

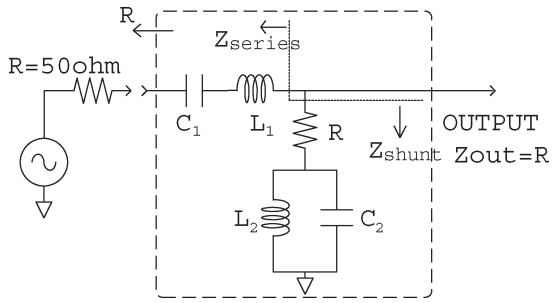

Fig. 3. Single stage of the BPF with constant output impedance and definition of $Z_{\rm shunt}$ and $Z_{\rm series}$.

apply an input signal $V_{\rm in}(t)$ to the device and obtain its output $V_{\rm out}(t)$, i.e.,

$$V_{\rm in}(t) = a\cos(\omega t)$$

$$V_{\rm out}(t) = b_0 + b_1\cos(\omega t) + b_2\cos(2\omega t) + b_3\cos(3\omega t) + b_4\cos(4\omega t) + b_5\cos(5\omega t) + \cdots$$

then its THD is defined as

$$\text{THD} = 10\log_{10}\frac{b_1^2}{b_2^2 + b_3^3 + b_4^2 + b_5^2 + \cdots}\ (\text{dB}).$$

If the power at the signal (carrier) frequency is A (dBm) and the power of a spurious component at interest is B (dBm), then

$$\text{the spurious component power} = A - B\ (\text{dBc}).$$

II. Principles of THD Measurement

A. THD Measurement System

Fig. 2 shows a diagram of our THD measurement system, wherein a pure sine wave signal is input to the DUT, and the output signal of the DUT is measured by a spectrum analyzer to detect the harmonic distortion that is generated in the DUT. Note that in Fig. 2, the THD is measured by the ratio of Vdis to A^*Vin, and in most cases, this ratio is very close to the ratio of Vdis to Vout.

Since state-of-the-art commercial signal generators have output harmonic distortion levels of about -60 dBc, we cannot directly use them as signal sources for high-resolution THD measurements. Thus, filters are required to remove the harmonics in the signal generator output, and the filters themselves must not generate additional distortion, to enable THD measurements over a wider dynamic range. A low-pass filter may be used for this purpose; however, a BPF is more desirable because it can remove low-frequency noise (e.g., power-line noise).

Also, the dynamic range of spectrum analyzers is typically about 80 dBc, which restricts the dynamic range of THD measurements. To overcome this limitation, we use a BEF between the DUT and the spectrum analyzer; this BEF suppresses only the carrier signal (the large signal component at the fundamental frequency, which is the same as the input signal frequency) while not affecting the level of very small sideband signals (harmonic components). This enables the spectrum analyzer to measure very small harmonic signals over a wide dynamic range. For the actual measurement, a low-noise amplifier was placed between the BEF and the spectrum analyzer to achieve the -130-dB-level measurement. This low-noise amplifier helps to reduce the equivalent noise level of the spectrum analyzer. Note that the low-noise amplifier does not need to have an extremely low THD because the largest component of the signal (i.e., the fundamental frequency component) is removed by the BEF. Hence, the low-noise amplifier does not significantly affect the distortion of the total measuring system; it only has to have a flat frequency response in the frequency range of interest.

B. BPF Design Concepts

In this subsection, we will explain the design concepts of the BPF that are used for the system in Fig. 2 [5]–[8]. To get enough attenuation at the frequency of the second harmonic distortion, we used a BPF of constant output impedance type with passive components (R, C, L). Fig. 3 shows a single stage of the BPF where

$$L_1 = L_2\ (= L), \quad C_1 = C_2\ (= C), \quad L = CR^2. \tag{1}$$

The overall BPF consists of several of these single-stage BPFs, which are connected in cascade. The single-stage BPF that is shown in Fig. 3 has the following characteristics.

1) Constant Resistive Output Impedance: The output impedance of this filter is constant throughout the entire frequency range (not only for the passband of the filter but also for the stopband of the filter), provided that we maintain the relationship among parameters (1) shown in Fig. 3; this enables us to connect many identical single-stage BPFs in cascade. Also, note that resistive termination does not affect the filter frequency response.

2) Low Q Value: The Q value of the circuit in Fig. 3 is relatively low; therefore, the circuit is tolerant of variations in component parameter values. However, the cascade connection of several stages enables the realization of a filter with sharp cutoff performance.

3) No Insertion Loss in the Passband (in Theory): In reality, there may be some loss, which is mainly caused by parasitic series resistance of inductors; however, this loss can be easily compensated for by calibration.

The impedance $Z_{\rm shunt}$ from each node to ground in Fig. 3 is given by the following:

$$Z_{\rm shunt} = R + \left(j\omega L_2 \| \frac{1}{j\omega C_2}\right) = \frac{R - \omega^2 LCR + j\omega L}{1 - \omega^2 LC}. \quad (2)$$

The series impedance $Z_{\rm series}$ from each node to the next node in Fig. 3 is expressed as follows:

$$Z_{\rm series} = R + j\omega L_1 + \frac{1}{j\omega C_1} = R + j\omega L + \frac{1}{j\omega C}. \quad (3)$$

Then, it follows from (1)–(3) that we have the following filter transfer function:

$$H_{\rm BPF}(j\omega) = \frac{Z_{\rm shunt}}{Z_{\rm series} + Z_{\rm shunt}} = \frac{(K\omega_0)j\omega}{\omega_0^2 + j\omega(\omega_0/Q) - \omega^2}. \quad (4)$$

Here

$$K = 1, \quad Q = 1, \quad \omega_0 = \frac{1}{\sqrt{LC}}. \quad (5)$$

We obtain from (4) and (5) that

$$H_{\rm BPF}(j0) = 0, \quad H_{\rm BPF}(j\infty) = 0, \quad H_{\rm BPF}(j\omega_0) = 1$$

and we see that the network in Fig. 3 is a BPF that is lossless in the passband. Also, we obtain from (1)–(3) that the network has a constant output impedance $Z_{\rm out}$, i.e.,

$$Z_{\rm out} = Z_{\rm series} \parallel Z_{\rm shunt} = R.$$

Remark: We may also generate a pure sine wave signal by using resonators that can be tuned to absorb the components of the harmonic distortion. In this method, most of the signal energy is not applied to the resonators, which may relax the requirements for the resonator components like L, C, and R. However, this method cannot remove unpredictable frequency components. For example, in case of an ADC evaluation, we have to detect not only the harmonic distortion but also spurious components like noise from the digital circuit portion, and the frequency of such spurious components may not correlate with the input signal frequency. Hence, the resonator filter cannot generate a pure signal without the spurious components. Because of this, the filter design concept described in Section II-B is superior to the concept described in this remark.

C. BEF Design

Our BEF shown in Fig. 4 is also designed using the same concepts as the BPF described in Section II-B, except that

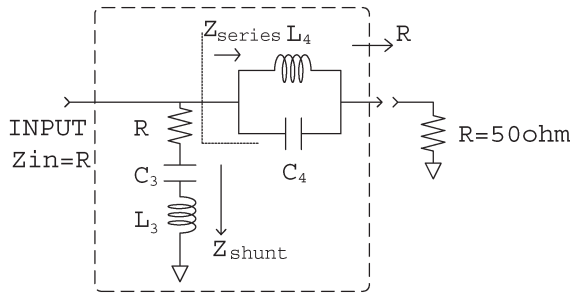

Fig. 4. Single stage of the BEF with constant input impedance and definition of $Z_{\rm shunt}$ and $Z_{\rm series}$.

it has constant input impedance. Similarly, we maintain the following:

$$L_3 = L_4\ (= L), \quad C_3 = C_4\ (= C), \quad L = CR^2. \quad (6)$$

The impedance $Z_{\rm shunt}$ from each node to ground in Fig. 4 is given by the following:

$$Z_{\rm shunt} = R + j\omega L_3 + \frac{1}{j\omega C_3} = R + j\omega L + \frac{1}{j\omega C}. \quad (7)$$

Also, the series impedance $Z_{\rm series}$ from each node to the next node in Fig. 4 is expressed as follows:

$$Z_{\rm series} = R + \left(j\omega L_4 \parallel \frac{1}{j\omega C_4}\right) = \frac{R - \omega^2 LCR + j\omega L}{1 - \omega^2 LC}. \quad (8)$$

Then, we have the following filter transfer function from (6)–(8):

$$H_{\rm BEF}(j\omega) = \frac{Z_{\rm shunt}}{Z_{\rm series} + Z_{\rm shunt}} = \frac{K\left(\omega_0^2 - \omega^2\right)}{\omega_0^2 + j\omega(\omega_0/Q) - \omega^2}. \quad (9)$$

Here

$$K = 1, \quad Q = 1, \quad \omega_0 = \frac{1}{\sqrt{LC}}. \quad (10)$$

We obtain from (9) and (10) that

$$H_{\rm BEF}(j0) = 1, \quad H_{\rm BEF}(j\infty) = 1, \quad H_{\rm BEF}(j\omega_0) = 0$$

and we see that the network in Fig. 4 is a BEF. Also, we obtain from (6)–(8) that the network has a constant input impedance $Z_{\rm in}$, i.e.,

$$Z_{\rm in} = Z_{\rm series} \parallel Z_{\rm shunt} = R.$$

Several BEF stages can be connected in cascade without affecting the input impedance.

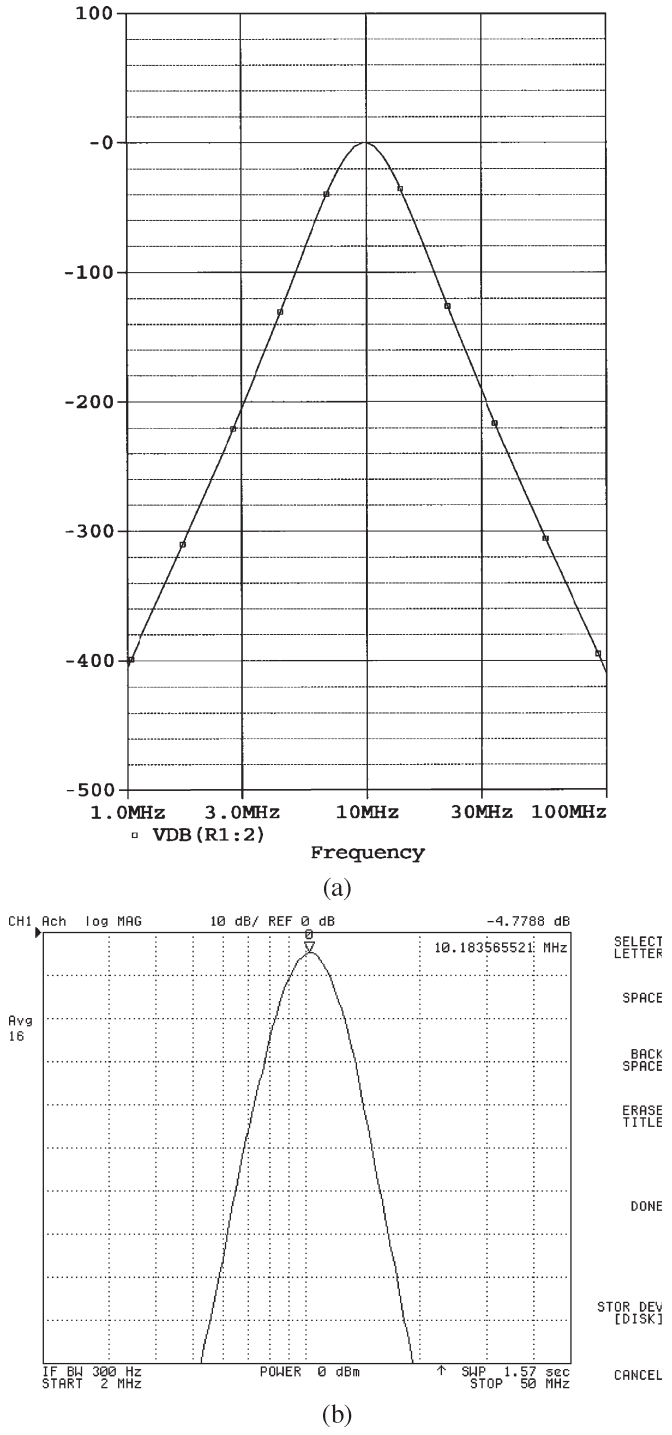

Fig. 5. Gain characteristics of the BPF with 20 stages with center frequency of 10 MHz. L = 0.82 uH, C = 318 pF, and R = 51 Ω. (a) SPICE simulation results. (b) Measurement results.

D. Actual Filter Implementation

For a 10-MHz BPF, 20 stages of the basic filter block described in Section II-B (Fig. 3) were connected in cascade, and the frequency response of this filter assembly was −100 dB at 20 MHz and −185 dB at 30 MHz. (However, it is very difficult to measure such low levels even when using state-of-the-art measuring equipment.) Fig. 5 shows SPICE-simulated and measured gain characteristics of our BPF with 20 stages.

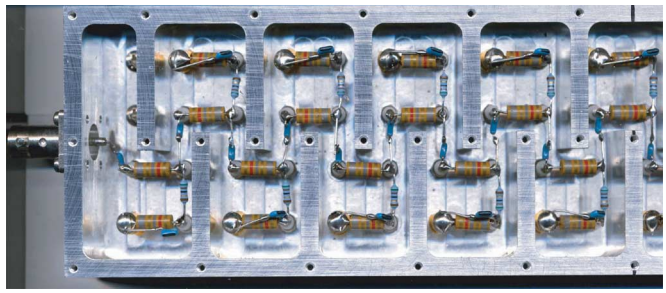

Fig. 6. BPF with 20 stages. Components of the filter are stud mounted in cavities of a cast-aluminum block. The holes shown in the photo are for screwing on the top cover.

We see in Fig. 5(b) that the measured gain at the center frequency is −4.8 dB (instead of 0 dB); this loss is due to parasitic resistances in L's and C's. Due to the high attenuation in the stopband, a pure sine wave signal can be extracted from a square wave input signal. The effectiveness of this concept is explained in Section III-C.

Remarks:

1) Quality of the parts used in the filter is very important. To achieve the expected frequency response, only the accuracy of components is a matter of concern; for distortion measurements, the distortion caused by filter parts is an additional concern. In most cases, the nonlinearity of magnetic cores of inductors causes distortion. We see clear nonlinearity such as saturation and hysteresis in typical B-H characteristics of the magnetic cores. Generally speaking, physically large inductors with low-permeability cores generate less distortion than small, for example, surface mount, inductors. Moreover, it is also true that high current in inductors causes high distortion; therefore, connecting inductors in parallel is an effective way to reduce distortion.
2) Mounting of the parts is also important. Any magnetic coupling between stages reduces attenuation in the stopband. To alleviate this problem, we mounted filter components in cavities of a cast aluminum block; such construction also helps minimize vibration-induced noise. Fig. 6 shows a photo of the BPF we have developed; the physical length of the BPF is 345 mm, the width is 75 mm, while the thickness is 28 mm.

The design of the BEF is similar to that of the BPF; however, in this case, a five-stage cascade connection is sufficient because the BEF only has to reduce the ratio between the fundamental signal and the harmonics to a level that the spectrum analyzer can handle. Fig. 7 shows the measured BEF gain characteristics with a five-stage cascade connection. The important parameter for the BEF is the frequency (gain) response at the second and third harmonic frequencies because, due to a low Q value of the BEF, the frequency response at those frequencies shows some attenuation. To precisely evaluate the levels of the second- and third-order harmonic distortion, we need to compensate for the measured frequency response of the BEF; we obtain the gain at the second harmonic frequency by measuring the BEF gain response with a network analyzer and adding the measured attenuation at the second harmonic

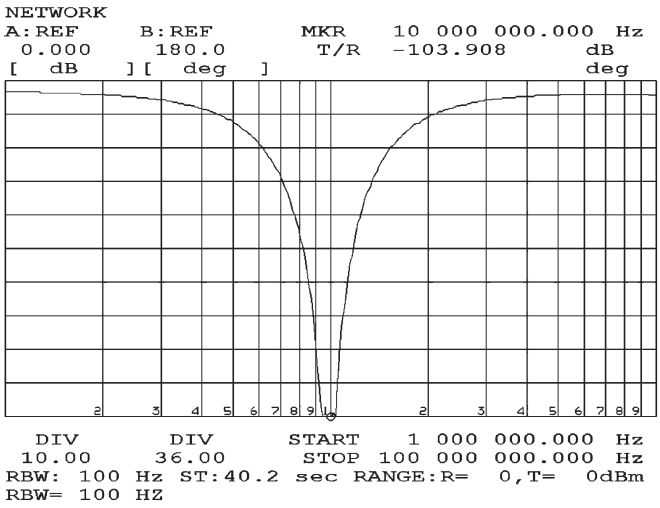

Fig. 7. Measured gain characteristics of the BEF with five stages with center frequency of 10 MHz.

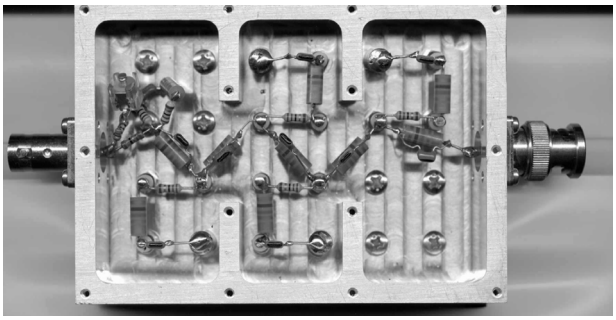

Fig. 8. BEF with five stages, with cover off.

frequency to the measured second harmonic power to compensate for the attenuation. Fig. 8 shows a photo of the BEF we have developed; the physical length of the BEF is 105 mm, the width is 75 mm, while the thickness is 28 mm.

We made seven kinds of filter sets with different center frequencies as described in Table I, and each filter has a fixed frequency response (not a variable frequency response). Table I shows the measured characteristics of the BPF and the BEF, which validate the performance of the design. The values in Table I are compensated for the attenuation of the BEF, and the overall performance was measured by directly connecting the BPF and the BEF. The signal voltage was measured with a resistive load of 50 Ω. Note that the signal level of 3Vp-p in Table I is large enough for present-day devices, and this value can be obtained with 50-Ω termination. The following are the reasons why the direct connection of the BPF and the BEF presents good results for the system evaluation.

1) If the distortion caused by the BPF could be completely canceled by the distortion caused by the BEF, their direct connection would show a very good THD performance. However, this would not happen because the number of stages for the BPF is different from that for the BEF; hence, an excellent measured THD performance (shown in Table I) for their direct connection means that the THD performance of both the BPF and the BEF are very good.

TABLE I
MEASURED CHARACTERISTICS OF SEVEN SETS OF BPF AND BEF USED IN THE THD MEASUREMENT SYSTEM

	center freq. f_c	BPF loss @f_c	BEF loss @$2f_c$	BEF loss @$3f_c$	overall 2nd-order distortion	overall 3rd-order distortion	overall signal range
No.	MHz	dB	dB	dB	dBc	dBc	Vp-p
1	1	-6.5	-13.4	-7.8	-143	-135	5.0
2	2	-5.0	-12.8	-7.6	-142	-146	5.0
3	5	-5.6	-11.4	-6.2	-146	-146	5.0
4	10	-4.8	-10.5	-5.7	-144	-142	5.0
5	20	-6.0	-10.4	-5.4	-136	-150	5.0
6	50	-6.3	-9.0	-5.0	-149	-153	3.1
7	100	-5.6	-12.2	-11.9	-143	-129	3.3

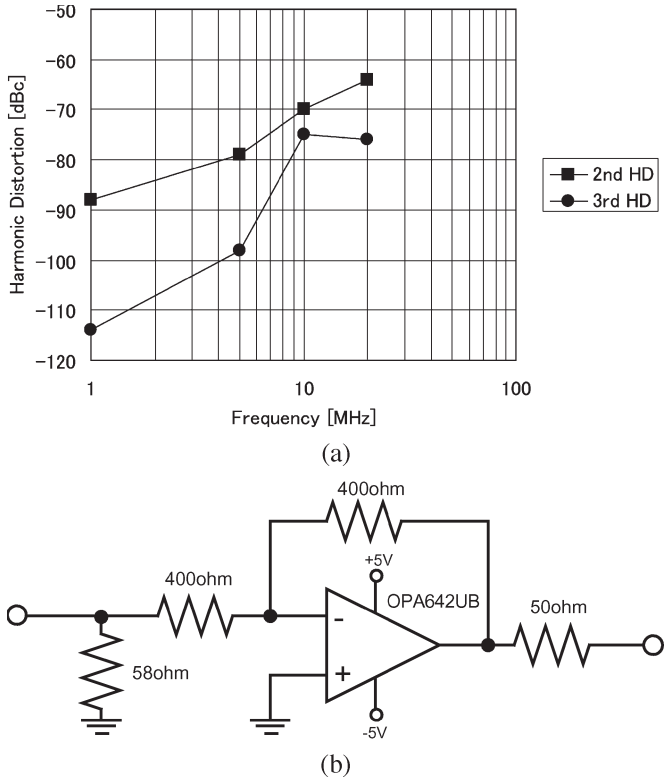

Fig. 9. (a) Measured distortion of an operational amplifier for input frequencies of 1, 5, 10, and 20 MHz. (b) Measurement configuration.

2) Before we achieved the performance that is described in Table I, we built a prototype system with −110-dBc-level performance. We can measure the performance of the prototype using the latest version of the BPF and the BEF with reasonable repeatability.

We describe other evidence that validates the performance that is achieved in Section III-D.

III. MEASUREMENT EXAMPLES WITH THE DEVELOPED SYSTEM

A. Operational Amplifier Distortion Measurement

The operational amplifier is the most popular analog device, and Fig. 9(a) shows the distortion measurement results of an operational amplifier (OPA642) using our measurement system with the configuration in Fig. 9(b) and a 10-dBm output.

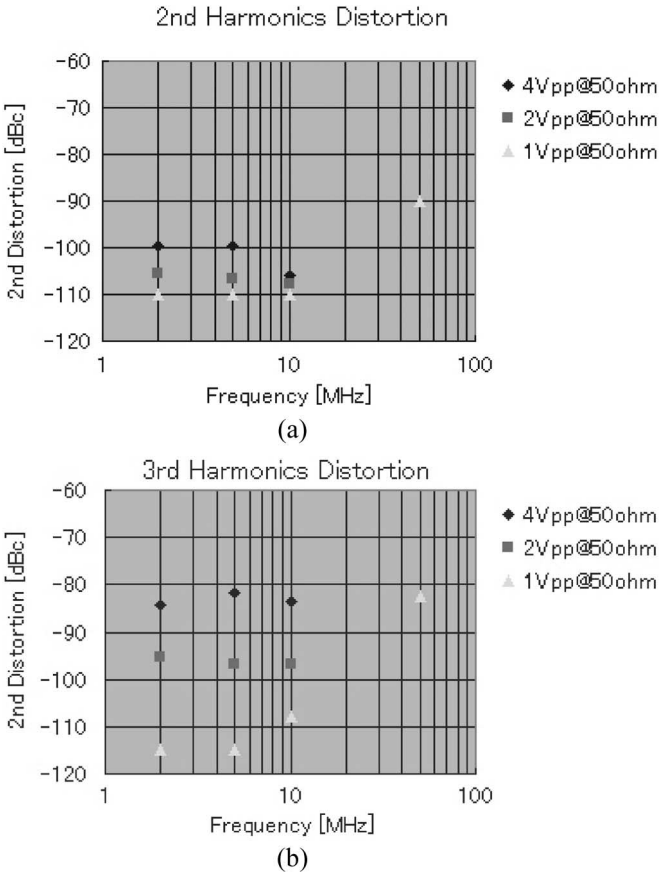

Fig. 10. Measured distortion of a photo MOS relay. (a) Second-order harmonic distortion. (b) Third-order harmonic distortion.

B. Photo MOS Distortion Measurement

Photo MOS relay switches are extensively used in automatic test equipment [large-scale integration (LSI) testers], which requires highly linear switches. For such applications, we evaluated the linearity of a photo MOS relay using our system; Fig. 10 shows its distortion measurement results.

The distortion level of the measured photo MOS relay is low enough for most applications in the automatic test equipment; we see in Fig. 10 that our proposed method clearly detects the distortion, whereas, to the best of our knowledge, other methods cannot detect such low distortion levels. Colleagues with material and fabrication expertise are now considering possible causes of the distortion, so the proposed system is helping them understand physics-of-materials phenomena.

C. Using Square Wave Signal as a BPF Input

For ADC performance measurement, we have to consider input signal phase noise [9]–[11], and we note that a BPF cannot remove the undesirable spectrum from a sinusoidal signal if the signal source has high levels of phase noise. It is widely known that, for signal sources with a high slew rate, voltage noise like thermal noise can be translated into phase noise. To keep the phase noise low, we need to treat fast transients like square waves. Therefore, we propose feeding a square wave from a quartz generator (whose phase noise is quite low) directly into

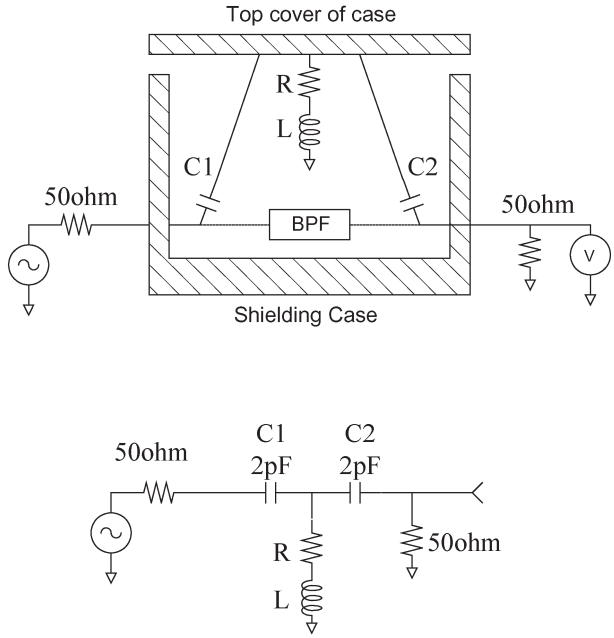

Fig. 11. Model of coupling between input and output of the BPF.

a BPF. As described in Section II-B, our proposed BPF can extract a pure sine wave from a square wave, and this scheme provides an acceptable phase noise performance. (We remark that a direct digital synthesizer may also be effective as the signal source that precedes the BPF [4].) However, realizing this concept is not easy because, theoretically, the third harmonic of a square wave is -10 dBc (which is rather large). To achieve a THD level of -130 dBc at the BPF output, we really need to attenuate third-order harmonics to -120 dB. A BPF with ten stages in cascade gives only -100-dB attenuation at the third-order harmonic frequency, even under ideal conditions (without any feedthrough). Therefore, we use 20 stages in series as the basic construction of the BPF. Furthermore, we need good isolation between the input and the output of the BPF, and hence, we use a rigid shielding case for mounting filter components. It is also important to keep the impedance of the top cover of the shielding case low. Fig. 11 shows a model for coupling between the input and the output of the BPF through the shielding case cover. To explain this by way of an example, let us assume that the center frequency of the BPF is 10 MHz, and calculate the attenuation at 30 MHz. Using the assumed value of parasitic components described in Fig. 11, L of 10 nH gives a -92-dBc level feedthrough at 30 MHz, whereas R of 0.2 Ω gives a -110-dBc level. Therefore, to achieve an attenuation of -120 dB, we have to keep these values low enough. In Figs. 6 and 8 (photos of the BPF and the BEF), we see many screw holes, which are prepared to keep the impedance of the cover low enough.

D. ADC With Wideband Sample/Hold Circuit

This subsection describes a data acquisition system using an A/D converter with a wideband sample–hold (S/H) circuit, and we propose a method for using our BPF to compensate for

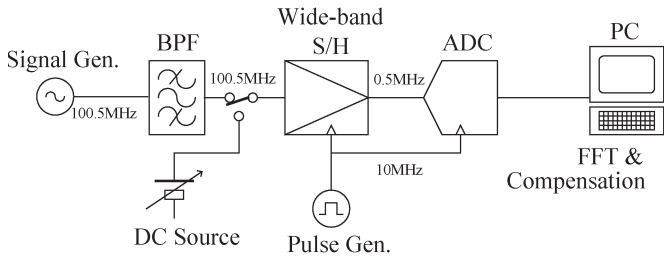

Fig. 12. ADC system configuration for the proposed distortion compensation.

the distortion of the ADC with an S/H circuit [12]. Fig. 12 shows the block diagram of the proposed method. Using our BPF to obtain a pure sine wave, we can measure the THD of the system by performing a fast Fourier transform (FFT) on the digital output data. (In this case, we use only the BPF and not the BEF because the DUT output is digital.) Fig. 13(a) shows the measurement results of ADC with a wideband S/H. The input signal frequency is 100.5 MHz, and it is generated through our BPF with the aforementioned method. Note that the 100.5-MHz signal is converted to about 500 kHz at the input of ADC by undersampling technology, with a sampling clock frequency of 10 MHz for S/H and ADC. In general, for an ADC with an S/H circuit, the measured distortion is the result of not only ADC and S/H nonlinearity but also input signal harmonics. However, since the above method with our BPF can create a pure sinusoidal input, almost all of the measured distortion is due to the DUT itself. Then, we measured the dc characteristics of the ADC with S/H by using a dc voltage source and a precision dc voltmeter to obtain a graph like Fig. 14. From this graph, we obtain a polynomial expression $(Y = a + bX + cX^2 + dX^3 + \cdots)$ that approximates the dc characteristics in Fig. 14. Then, we apply the signal under test to the ADC with S/H and also apply the reverse function of the polynomial expression to the captured digital data to cancel its nonlinearity and obtain $Y = a + bX$; the linearity of the ADC can be improved by digital data processing.

Fig. 13 shows the effectiveness of the proposed linearity compensation method for the ADC with an S/H circuit. Fig. 13(a) shows the measured output spectrum (obtained by an FFT of the ADC output data) of the ADC with an S/H circuit for the 100.5-MHz sinusoidal input signal, whereas Fig. 13(b) shows the spectrum after compensation. We see that applying this compensation method reduces the THD level of the 100.5-MHz signal by 18 dB.

In this case, the data for compensation were taken through the dc characteristics measurement, which means that the main cause of distortion in the system at 100.5 MHz is the same as that at dc; this relationship between ADC dc linearity and ac linearity at 100.5 MHz is one of the wideband application examples described in Section I. We remark that this compensation method would also be applicable to the A/D conversion of complex signals in I/Q modulation. We would like to close this section by remarking that a complete validation of the -130-dBc-level performance achievement of our THD measurement system is very difficult. Therefore, we tried several methods to obtain the evidence that validates the achievement of the -130-dBc-level THD measurement performance.

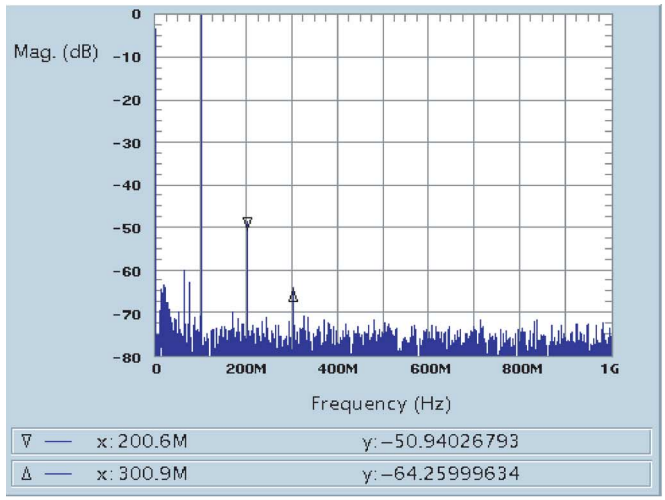

(a)

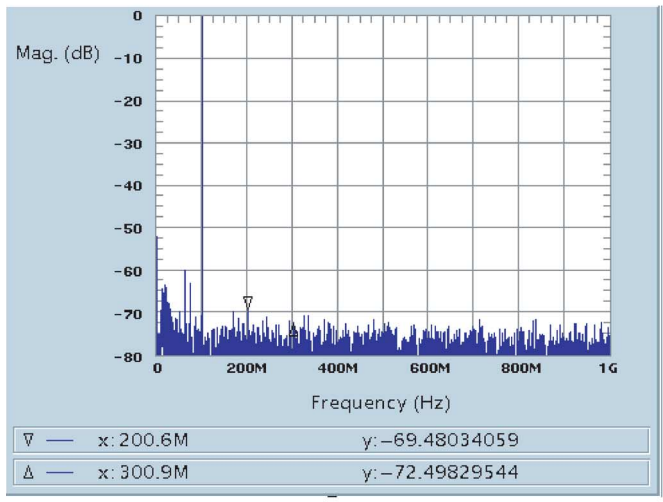

(b)

Fig. 13. Measured distortion of an ADC with an S/H circuit. (a) THD $= -48.5$ dBc at 100 MHz without compensation. (b) THD $= -66.8$ dBc at 100 MHz with the proposed compensation.

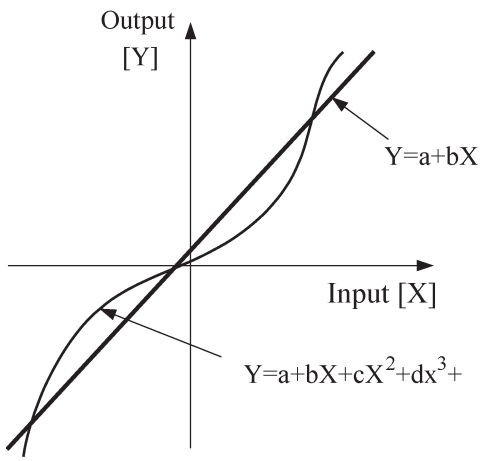

Fig. 14. Principle of the proposed linearity improvement method for an ADC with an S/H circuit.

1) In Section II-B (in Table I), we showed THD performance validation results with the direct connection of the BPF and the BEF.
2) In this section, we showed the relationship between the ac linearity of the BPF and the dc linearity compensation based on a different principle from that in Section II-B, and the very good ac linearity of our BPF is partially proven through this compensation method. Note that it is impossible to confirm the linearity of the BPF by simple dc measurements as the BPFs do not pass dc.

Through our extensive experiments, we did not find anything that disproved that we have achieved the performance of −130-dBc level.

IV. Conclusion

We first described the importance of THD measurement of electronic devices at frequencies higher than typical audio applications with several examples, and then, we proposed a THD measurement system that can measure the THD of analog input and/or analog output devices like operational amplifiers, ADCs, and DACs at frequencies of several tens of megahertz. The proposed system uses the passive BPF and BEF, and we described their design, implementation, and measured performance. The proposed system can measure THD components down to −120 dBc or less over a frequency range from 1 to 100 MHz, which has not been achieved with other methods [we believe that this performance will be sufficient for our next-generation automatic test equipment (LSI tester) applications]. By paying attention to component selection and mounting, we have created a mechanically sturdy measurement system with good reliability and repeatability. We have described examples of THD measurement that verify the effectiveness of using the proposed system. This system is now being intensively used for evaluating our electronic measurement instrument products.

This paper has shown us that new knowledge can be gained even by researching classical subjects like THD measurement or passive filters at a deeper level than ever before, and we conclude this paper by remarking that, in addition to its electrical applications, this system has the potential to be used as a very sensitive detector of physical phenomena with parts-per-million-level resolution.

Acknowledgment

The authors would like to thank their managers for the encouragement to publish the technical contents described here. They would also like to thank their colleague H. Kakitani for careful experiments that obtained valuable data, as well as K. Wilkinson for improving the manuscript.

References

[1] B. Metzler, *Audio Measurement Handbook*, 2nd ed. Beaverton, OR: Audio Precision, 2005.
[2] *HP 8903B Audio Analyzer Operation and Calibration Manual*, Hewlett-Packard, Spokane, WA, 1989.
[3] *APWIN System Two Cascade User Manual*, Audio Precision, Beaverton, OR, 2001.
[4] P. Wambacq and W. Sansen, *Distortion Analysis of Analog Integrated Circuits*. Norwell, MA: Kluwer, 2002.
[5] *The Circuits and Filters Handbook*, 2nd ed. W.-K. Chen, Ed. Boca Raton, FL: CRC, 2003.
[6] R. Scahumann and M. Valkenburg, *Design of Analog Filters*. London, U.K.: Oxford Univ. Press, 2001.
[7] L. D. Paarmann, *Design and Analysis of Analog Filters*. Norwell, MA: Kluwer, 2001.
[8] M. Valkenburg, *Analog Filter Design*. New Delhi, India: CBS, 1982.
[9] M. Shinagawa, Y. Akazawa, and T. Wakimoto, "Jitter analysis of high-speed sampling systems," *IEEE J. Solid-State Circuits*, vol. 25, no. 1, pp. 220–224, Feb. 1990.
[10] H. Kobayashi, K. Kobayashi, M. Morimura, Y. Onaya, Y. Takahashi, K. Enomoto, and H. Kogure, "Sampling jitter and finite aperture time effects in wideband data acquisition systems," *IEICE Trans. Fundam.*, vol. E85-A, no. 2, pp. 335–346, Feb. 2002.
[11] N. Kurosawa, H. Kobayashi, H. Kogure, T. Komuro, and H. Sakayori, "Sampling clock jitter effects in digital-to-analog converters," *Measurement*, vol. 31, no. 3, pp. 187–199, Mar. 2002.
[12] T. Komuro, S. Sobukawa, H. Kobayashi, and H. Sakayori, "THD measurement and compensation for analog circuits with fine CMOS devices," in *Proc. Int. Conf. Solid-State Devices Mater.*, Kobe, Japan, Sep. 2005, pp. 664–665.

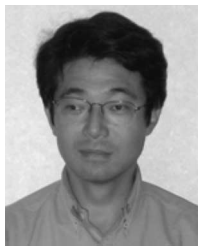

Takanori Komuro (M'85) received the B.S. degree from Tokyo University, Tokyo, Japan, in 1985. He received the Ph.D. degree from Gunma University, Kiryu, Japan, in 2007, where he is currently a Guest Professor.

He joined Yokogawa Electric Corporation, Tokyo, in 1985. After working at the Superconductivity Sensor Laboratory, he joined Hewlett-Packard Japan in 1997, where he was engaged in research and development of test equipment of semiconductor devices. He is currently with Agilent Technology International, Hachioji, Japan. His current interests are in analog circuits for test and measurement equipment.

Shingo Sobukawa received the B.S. degree from Aichi Institute of Technology, Aichi, Japan, in 1980.

He joined NF Corporation, Yokohama, Japan, in 1980, where he has been engaged in the design and development of many preamplifier products such as SA-230F5 ($G = 46$ dB, $F = 1$ k to 100 MHz, and NF $= 0.6$ dB at 50 Ω, 10 MHz).

Hiroshi Sakayori received the B.S. degree in electronic engineering from Waseda University, Tokyo, Japan, in 1972.

He joined Agilent Technologies Japan Ltd. (formerly Yokogawa Hewlett-Packard) in 1972, where he developed LCR meters, related products, and semiconductor test equipment and systems. From 1992 to 1997, he temporarily left Agilent Technologies and joined a consortium, where he took part in developing high-speed data conversion technology. He is currently with Agilent Technology International, Hachioji, Japan.

Mr. Sakayori is a member of the Institute of Electrical Engineers of Japan.

Masashi Kono (S'03) received the B.S. and M.S. degrees in electronic engineering in 2003 and 2005, respectively, from Gunma University, Kiryu, Japan, where he is currently working toward the Ph.D. degree.

His research interests are MEMS, switching regulators, analog integrated circuit design, and measurement technologies.

Mr. Kono received the Young Researcher Encouragement Award from the Institute of Electrical Engineers of Japan in 2003.

Haruo Kobayashi (S'88–M'89) received the B.S. and M.S. degrees in information physics from the University of Tokyo, Tokyo, Japan, in 1980 and 1982, respectively, the M.S. degree in electrical engineering from the University of California, Los Angeles, in 1989, and the Dr. Eng. degree in electrical engineering from Waseda University, Tokyo, in 1995.

He joined Yokogawa Electric Corporation, Tokyo, in 1982, where he was engaged in research and development related to measuring instruments and minisupercomputers. From 1994 to 1997, he was involved in research and development of ultrahigh-speed ADCs/DACs at Teratec Corporation. During this period, he was also an Adjunct Lecturer with Waseda University. In 1997, he joined Gunma University, Kiryu, Japan, where he is currently a Professor with the Electronic Engineering Department. His research interests include mixed-signal integrated circuits design and signal processing algorithms.

Mr. Kobayashi received the Best Paper Award from the Japanese Neural Network Society in 1994 and the Yokoyama Award in Science and Technology in 2003.